Kuwait J. Sci. 46 (1) pp 76-83, 2019

Steady-state performance investigation of closed-circuit hydrostatic system: A practical approach

Ajit Kumar Pandey*, K. Dasgupta, N. Kumar
Dept. of Mining Machinery Engineering, IIT (ISM), Dhanbad - 826004, Jharkhand, India
**Corresponding author: ajit.saurabh100@gmail.com*

Abstract

The steady-state performance of a hydrostatic (HST) drive through modelling and experiment. was investigated. The drive had a closed-circuit configuration, in which the supply from the variable displacement pump drives a variable displacement hydro-motor. The aim was to demonstrate the torque-speed control of the hydrostatic drive by varying the pump or motor displacements with respect to the overall efficiency, torque-loss (%), and slip. The bond graph simulation technique was used to model the HST drive, where the losses of the pump and hydro-motor are lumped through resistances. The characteristics of the losses were identified through test-data. The drive's performance was studied with respect to the variation of the pump and the hydro-motor displacements. The investigation identifies the efficient zone of operation for these drives. Design engineers and manufacturers will find the results useful, particularly when adapting control guidelines of hydrostatic drives used for mining application.

Keywords: Efficiency; hydrostatic drive; motor displacement ratio; pump displacement ratio; slip; torque loss.

1. Introduction

A hydrostatic (HST) drive is used in heavy earth moving machineries (HEMMs) for its high-power density, wider speed-torque range, better controllability and excellent steady-state as well as dynamic performances. Such drives used to propel HEMM mainly have a closed-circuit configuration. In this setup, the pump and hydro-motor are directly connected without additional losses. Conventional HST drives often utilize a variable displacement pump with a fixed displacement hydro-motor (Zarotti & Nervegna, 1983; McCandlish, & Dorey, 1984; Watton, 2005). In such a drive, the hydro-motor speed is proportional to the pump flow rate. However, in the closed circuit drive where both the pump and the hydro-motor are variable, the drive speed can be further increased by adjusting the hydro-motor displacement to lower values. This is due to the fact that motor speed is inversely proportional to its displacement. The overall efficiency of a mobile drive concept is a result of the power output and losses in every single sub-system. Therefore, losses in the hydrostatic components have significant influence on the performance of the HST drive (Mandal *et al*., 2009; Williamson & Ivantysynova, 2007; Rahmfeld & Skirde, 2010). In recent decades, various analytical, physical, power and numeric approaches have been suggested to describe the losses, these are based on quasi-static measurement results (Conrad *et al*., 1993; Lux & Murrenhoff, 2016; Kohmäscher *et al*., 2007). Hasan *et al.* (2015) have compared the performance of four types of open-circuit high-speed low-torque hydrostatic drives using a bent-axis fixed displacement motor. Research shows that a hydrostatic drive using speed controlled pump exhibits maximum efficiency. This analysis does not consider the losses of the drive that depends on the displacement of the pump. Khorshid & Gad (2006) analytically studied the steady-state and dynamic performance of the servomotor. They compared the predicted data obtained through modeling with test data. They concluded that the neural network technique applied to the servomotor model is suitable for a transient mode of operation of highly non-linear systems. The performance predictions of roadheaders used in underground mining has been studied by Özfırat *et al.* (2017). The effects of several factors on the roadheader's performance were examined. These included the power of the machine, weight of the machine, power to weight ratio, drilling rate index, uni-axial compressive strength, and the rock mass rating. The machine performance was found to be highly correlated with the machine power (P), weight (W) and the P/W ratio. The selection of optimal technology for surface mining was studied by Stojanovic *et al.* (2015). The authors demonstrated different methods for selecting optimal technology using an open pit coal mine. The study investigated mining-technical factors, including equipment utilized, systems, etc. None of previous studies analyzes the combined performance of the pump and the motor in an HST drive used in mining applications. In this study, the performance characteristics of a closed-circuit hydrostatic drive is investigated. The focus is on the wider range of torque-speed by operating it under different modes. In the pump-controlled mode, pump displacement is varied, while keeping motor displacement fixed. For the motor controlled, motor displacement is varied while pump displacement is kept fixed. The performance of the drive has been investigated for a wide torque–speed range in terms of the overall efficiency (η), slip, and torque loss (%) In

investigating the performance of the HST drive, a pragmatic approach is followed to estimate its various losses due to complicated flow mechanics involved in the components. The data contributes to the development of design guidelines. Components of the HST drive for mining application could be selected without developing a prototype for the test data. The bases for selecting the best combination of the pump and motor of an HST drive are critical parameters in regards to overall efficiency (η), displacement ratios of the pump (β_{pd}) and the motor (β_{md}), and load torque (τ_{ld}). Also discussed are the effects of variation of β_{pd} and β_{md} on the drive's performance. In analyzing the drive's performance, modeling of the system is made using bondgraph simulation technique (Thoma, 1990). In this case, the pump and motor losses are represented by suitable resistances. Their non-linear characteristics that depend on the state-variables of the drive were identified experimentally. The overall performance of the HST drive is examined with respect to its different performance parameters. In this paper, the steady-state model is presented. This model guides the design of the experiment and mode of observation data handling in such a way that the dependency of the parameters on the HST drive pump and motor operating conditions are obtained.

2. Physical system

The schematic representation of the closed-circuit HST drive considered for analysis is shown in Figure 1(a).

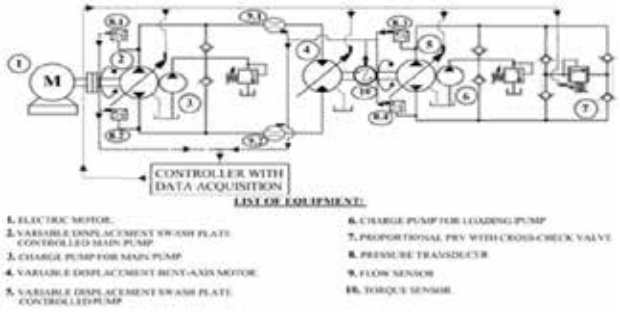

Fig. 1(a). Schematic diagram of the closed-circuit HST drive

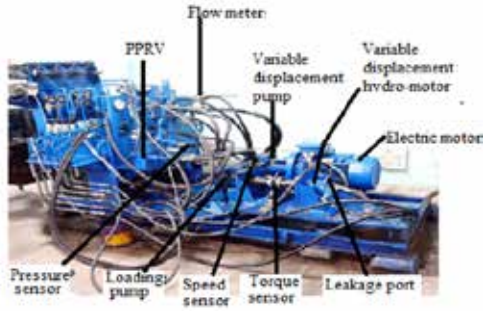

Fig. 1(b). Pictorial view of the test rig of the closed-circuit HST drive

Figures 1(a) and 1(b) give the schematic and pictorial representations of the experimental test rig of the hydrostatic drive, respectively. The main component used in the test-rig with a specification summary are listed in Table 1.

Table 1. List of major component used in the test-rig.

Item. No.	Name and Specification	Make and Model
1	3-Phase induction motor Power-15 KW Speed 1450 RPM	NADJ40224HTOP Compton Greaves Ltd.
2	Variable displacement pump Maximum displacement 28 cc/rev	A4VG28EP2DM1/3XRPZC10F 02D/Bosch Rexroth, Germany
4	Variable displacement hydro-motor Maximum displacement 28 cc/rev	A2FM16/61W-VBB030/ Bosch Rexroth, Germany
5	Variable displacement swash plate controlled loading pump Maximum displacement 28 cc/rev	A4VG28EP2DM1/3X– RPZC10F02D/ Bosch Rexroth, Germany
8.1 through 8.4	Pressure sensor Accuracy- 0.25 % Pressure range- (0-200 bar)	S10/Wika, Germany
9.1 through 9.2	Flow sensor Turbine type flow sensor Accuracy ±0.5% Flow range-0-60 LPM	TFM 1015/Rockwin Flow meter India Pvt. Ltd
10	Torque sensor Accuracy- 1% of full scale torque Max. torque range- 100 Nm	K-T40B-100Q-MF-S-M-DU2-0-S/ HBM, Germany

Referring to Figure 1(a), the main features of the test-rig are as follows:

a) An electric motor (1) drives a variable displacement pump (2) at a constant speed. The pump supplies pressurized fluid to the inlet of the variable displacement bent-axis hydro-motor (4).
b) The hydro-motor (4) in turn drives an identical pump (5) in the loading circuit that supplies pressurized fluid to the proportional pressure relief valve (PPRV) (7).
c) The controller gives a command signal that varies from 0-10-volt DC to adjust the displacement of the pumps, hydro-motor and the set pressure of the PPRV for a targeted speed and torque output of the drive.
d) Similarly, the load on the hydro-motor is controlled by adjusting the swash plate angle of the pump or the pressure setting of the relief valve.
e) The charge pumps (3 and 7) compensate leakage losses. For a detailed functioning of the component, refer to the standard textbook by Watton (2009).
f) The sensors and digital indicators record parameters such as pressure (8), flow (9), and rotational speed as well as torque (10).

During the experiment, the hydraulic oil temperature and other fluid properties were kept constant as much as possible. Leakage flow is assumed to be directly proportional to the working pressure difference. Care has been taken to keep the pressure difference constant during measurements. The pressure, flow, torque and the speed sensors were

set to appropriate levels following the standard method (Ivantysyn & Ivantysynova, 2002) and were calibrated to collect the test data. The experiments were conducted for the drive speeds from 400 rpm to 2400 rpm. Load torque and operating pressure varied from 28 Nm to 50 Nm and 63 bar to110 bar, respectively. The experiments could not be performed at a higher torque setting due to set-up limitations. Repeated test runs were made following the standard test procedure (BS 4617, 1983).

3. Modeling of the system

The following were taken into consideration while developing the steady-state model of the system:

- The effects of the resistance and the capacitance of the hydraulic fluid flow passage are lumped, wherever appropriate.
- Line resistance is not taken into account.

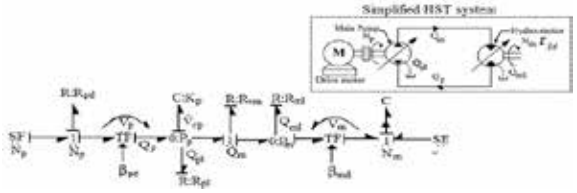

Fig. 2. Steady-state bond graph model of simplified HST drive

Figure 2 shows the bond graph model of the simplified HST system. A hydraulic displacement machine translates hydraulic power into mechanical power or vice-versa. The pump and the motor displacement ratios (β_{pd} and β_{md}) are represented by the respective modulated transformer (TF) junctions. In the model, the SF element with the junction represents the speed (N_p) of the pump. The total mechanical loss of the pump is presented by the resistive element R_{pd} attached at the 1_{N_p} junction. This is done by combining the pressure drop across the valve ports of the pump (originating from fluid flow) with the frictional loss. Similarly, the valve-port resistance of the motor R_{vm} on the junction represents the torque-loss of the hydro-motor. The resistance R_{pl} on the pump plenum junction represents resistance to the pump leakage. The C element on the same junction indicates the bulk stiffness of the hydraulic fluid K_{cp}. The pump supplies flow Q_p through the inlet port to the motor plenum, represented by junction. The resistance Rml represents the motor's leakage. The hydro-motor transforms the hydraulic power to mechanical power that drives the load (τ_{ld}). The SE element on the 1_{Nm} junction, which represents the opposing load torque, determines the differential pressure across the motor (P_m). The C element attached to the same junction observes the motor speed (N_m). The transformer moduli V_p and V_m indicate the pump and the motor volumetric displacements, which depend on the displacement ratios (β_{pd} and β_{md}). These are expressed as $V_p = \beta_{pd} V_{p\,max}$ and, $V_m = \beta_{md} V_{m\,max}$ where $V_{p\,max}$ and $V_{m\,max}$ are maximum volume displacement of the pump and the hydro-motor, respectively. Their values are taken from the manufacturer's product catalogue (Bosch Rexroth)The system equations are obtained from the steady-state model developed by using the bond graph simulation technique, where the loss coefficients are experimentally identified.Referring to Fig. 2, the steady-state flow supplied to the plenum of the hydro-motor is given by:

$$Q_m = Q_p - Q_{pl} \tag{1}$$

where, the second term represents the ideal pump flow, $(Q_p) = N_p \beta_{pd} V_{p\max}$, and the third term represents the pump leakage flow $Q_{pl} = \frac{P_p}{R_{pl}}$.

The leakage resistance of the pump is expressed as:

$$R_{pl} = \frac{P_p}{Q_{pl}} \tag{2}$$

Similarly, the flow rate through the inlet valve port of the hydro-motor is expressed as:

$$Q_m = \frac{(P_p - P_m)}{R_{vm}} \tag{3}$$

Also, the valve-port resistance at the inlet of hydro-motor is given by:

$$R_{vm} = \frac{(P_p - P_m)}{(N_p V_p - \frac{P_p}{R_{pl}})} \tag{4}$$

The leakage flow of the motor may also be written as:

$$Q_{ml} = \frac{\tau_{ld}}{V_m R_{ml}} \tag{5}$$

The leakage resistance of hydro-motor is given as:

$$R_{ml} = \frac{\tau_{ld}}{V_m Q_{ml}} \tag{6}$$

Finally, the predicted pump torque is given by:

$$\tau_{pp} = P_p V_p + R_{pd} N_p \tag{7}$$

From Equation (7), the pump drag resistance is given as:

$$R_{pd} = (\tau_{pp} - P_p V_p) / N_p \tag{8}$$

The actual slip of the HST drive is expressed as:

$$S_a = \frac{N_{mi} - N_{ma}}{N_{mi}}, \tag{9}$$

where the hydro-motor's ideal speed N_{mi} reads:

$$N_{mi} = \frac{N_p V_P}{V_m} \tag{10}$$

Actual torque loss may be expressed as:

$$\Delta\tau_{la} = \tau_{pa} - \tau_{ld} \tag{11}$$

The actual overall efficiency of the drive is given by:

$$\eta_a = \frac{N_{ma} \tau_{ld}}{\tau_{pa} N_p} \tag{12}$$

The test data obtained through different sensors described in section 2 are used in Equations (9, 11, and 12) to calculate the values of actual slip, torque-loss and efficiency. These are compared with corresponding predicted values. The expressions for predicted slip, torque-loss and efficiency are given in Appendix 1. The abbreviations of the notations and

their significance are also mentioned in Appendix 2.

4. Experimental outcomes and discussion

By varying the displacements of the pump and the hydro-motor in the pump- and motor-controlled modes of operation, the performances of the drive was tested for load torque and drive speed ranges of 28-50 Nm and 400-2400 rpm, respectively. However, due to test set-up limitations, the displacement of the pump (V_p) and the hydro-motor (V_m) could not be lowered below 40% of its maximum value. The maximum pressure level was achieved up to 120 bar. During the experiment, the fluid temperature was maintained to $50\,^0C \pm 2$. The pressure difference across the hydraulic machine was kept constant with reasonable accuracy during the experiment. Repeated test runs were made following the standard test procedure (BS 4617, 1983).

4.1 Pump and hydro-motor loss estimates

The test data for flow rate, pressure across the pump and motor, their speed and their torque were obtained from the respective sensors. The results were input into Eqaution (2), (4), (6), and (8) in order to obtain pump and the motor loss coefficients.

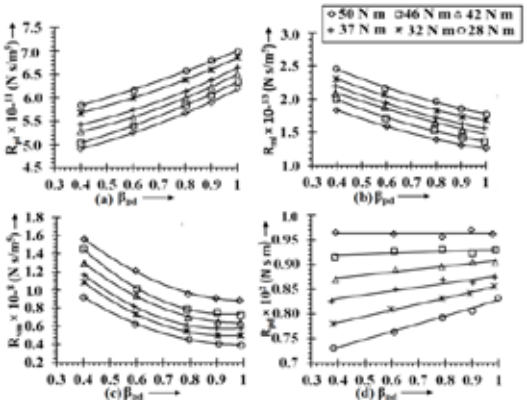

Fig. 3. Characteristics of the pump and hydro-motor losses as a function of β_{pd}

The variation of the loss coefficients R_{pl}, R_{ml}, R_{vm} and R_{pd} with respect to the βpd and βmd are shown in Figures (3) and (4), respectively. The characteristics of these loss coefficients are obtained from best fit curves lines to the data points. The polynomials for the R_{pl}, Rml, Rvm and Rpd with respect to the pump and the motor displacements ratio are expressed in Appendix 3.

- From Figures 3(a) and 4(a), it is observed that by increasing β_{pd} or β_{md}, leakage resistance of the pump (R_{pl}) increases. Also, at a constant β_{pd} and β_{md}, with rising load torque levels, Rpl decreases in both modes of operation.
- The leakage resistance of the hydro-motor R_{ml} reduces with the raise in β_{pd}; whereas R_{ml} increases with increase in β_{md} as shown in Figures 3(b) and 4(b). At a constant β_{pd} and β_{md}, with rising load torque levels, Rml also decreases in both modes of operation.
- Figures 3(c) and 4(c) indicate the characteristics of the motor valve port resistance R_{vm}. It is observed that R_{vm} decreases with the rise in the βpd, whereas R_{vm} increases with increase in β_{md} for the same load torque. Also, R_{vm} increases with increase load torque at the constants β_{pd} and β_{md}, which translates into torque-loss. Increase in Rvm increases torque loss and decreases torque loss percentage.
- From Figures 3(d) and 4(d), it is found that pump drag resistance Rpd rises with the rise in the β_{pd}. However, it decreases with the increase in β_{md} for the same load torque. R_{pd} rises with the rise in the load torque at fixed β_{pd} and β_{md}. An increase in R_{pd} reduces the mechanical efficiency of the pump.

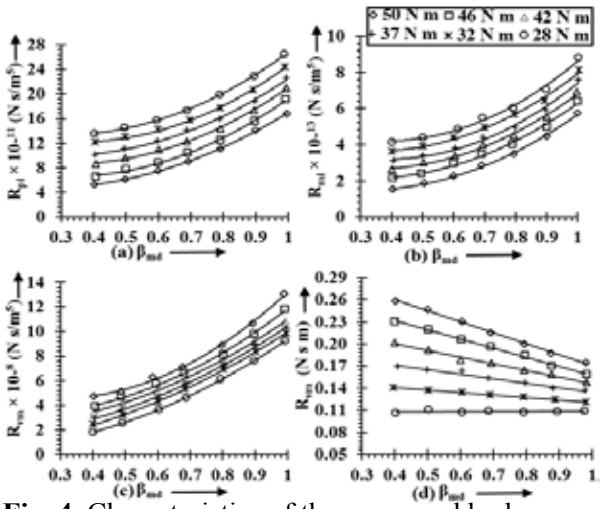

Fig. 4. Characteristics of the pump and hydro-motor losses as a function β_{md}

A similar trend of the resistances given were found in McCandlish & Dorey (1984) and Mandal *et al*. (2009) in their investigation on the plunger type hydro-static unit. The variation of R_{vm} described by the quadratic relationship was also observed (Thoma, 1969).

4.2 Performance parameters of the HST drive

The performance parameters, such as the torque-loss (%), slip and efficiency of the HST drive, are examined with respect to the β_{pd} and the β_{md} in pump-and motor-controlled modes, respectively.

4.2.1 Slip behaviour of the HST drive

Leakage flow of the pump and hydro-motor translates into the drive's slip. Equations (9) and (23) are used to calculate and compare the actual and the predicted slip as shown in Figure 5. Figure 5 shows the slip behaviour of the HST drive. It can be observed that:

1. In the pump controlled-mode of operation, the slip reduces with the rise in drive speed for a particular torque level, which is caused by an increase in the R_{pl} at higher β_{pd}.

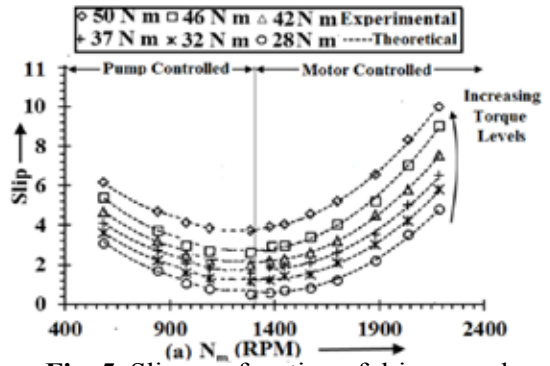

Fig. 5. Slip as a function of drive speed

2. In the motor controlled-mode of operation, the slip increases with the rise in drive speed for a particular torque level, which is due to a decrease in the R_{ml} at lower β_{md}.
3. Higher slip losses occur when the load torque increases at a fixed value of βpd or βmd, which is mainly due to the decrease in Rpl and Rml (see Figures 3(a), 3(b), 4(a), and 4(b)). In general, slip increases with increasing torque for both modes of drive operation.
4. At a constant torque-level, when there is an increase in β_{pd}, the slip decreases, whereas a decrease in β_{md} increases the slip of the drive.

Table 2. Actual and theoretical values of the slip of the drive at different load torque.

T_{ld}=28 N m			T_{ld}=32 N m			T_{ld}=37 N m		
N_m (RPM)	S_a	S_p	N_m (RPM)	S_a	S_p	N_m (RPM)	S_a	S_p
588	3.1	3.2	590	3.6	3.7	595	4.1	4.1
839	1.7	1.8	859	2.2	2.3	852	2.7	2.8
984	1.1	1.2	987	1.5	1.7	984	2.2	2.2
1100	0.7	0.7	1096	1.3	1.3	1100	1.8	1.8
1293	0.4	0.5	1292	1.1	1.2	1297	1.7	1.8
1386	0.4	0.6	1386	1.1	1.4	1387	2.0	2.1
1458	0.6	0.7	1460	1.3	1.5	1455	2.2	2.2
1588	0.6	0.8	1569	1.4	1.6	1580	2.5	2.6
1700	1.1	1.3	1706	2.0	2.2	1703	3.2	3.2
1883	2.0	2.1	1884	3.1	3.2	1887	4.5	4.5
2042	3.3	3.5	2031	4.2	4.2	2047	5.0	5.2
2212	4.5	4.8	2184	5.7	5.8	2179	6.4	6.5
2332	5.6	6.2	2307	6.7	6.9	2318	7.7	7.7
2400	6.7	7.1	2400	7.9	8.0	2400	8.6	8.7
T_{ld}=42 N m			T_{ld}=46N m			T_{ld}=50 N m		
N_m (RPM)	S_a	S_p	N_m (RPM)	S_a	S_p	N_m (RPM)	S_a	S_p
592	5.3	5.3	595	4.7	4.8	592	6.1	6.2
855	3.6	3.7	847	3.0	3.1	846	4.6	4.7
981	2.9	3.2	992	2.4	2.5	981	4.0	4.1
1100	2.6	2.9	1104	2.2	2.3	1094	3.7	3.8
1297	2.6	2.7	1292	1.9	2.2	1293	3.6	3.7
1387	2.8	2.9	1384	2.1	2.2	1384	3.8	4.0
1468	2.8	3.0	1460	2.1	2.4	1452	4.0	4.0
1587	3.3	3.4	1576	2.5	2.6	1577	4.5	4.7
1716	4.0	4.0	1705	3.1	3.2	1703	5.1	5.3
1887	5.1	5.4	1888	4.4	4.5	1887	6.4	6.6
2050	6.9	7.3	2043	5.7	5.9	2044	8.1	8.2
2189	9.0	9.0	2195	7.5	7.5	2196	9.9	9.9
2315	10.4	10.4	2319	8.8	8.9	2312	11.6	11.7
2400	11.7	11.8	2400	10.0	10.1	2400	12.7	12.9

4.2.2 Torque-loss performance of the HST drive

The R_{vm} and R_{pd} are the major influencing parameters for the torque loss of the drive. Such losses translate into mechanical efficiency of the HST drive. Figure 6 compares the predicted torque-loss characteristics of the drive with the test-data obtained from Equations (11) and (16). From Figure 6, it is observed that:

1. At a constant load torque, with an increase in pump and motor displacements (β_{pd} and β_{md}), the percentage of torque loss increases. This is due to the fact that as βpd increases, the speed increases. R_{pd} also rises (Figure 3(d)). R_{pd} increases with an increase in βpd Nm (Figure 3(d)).

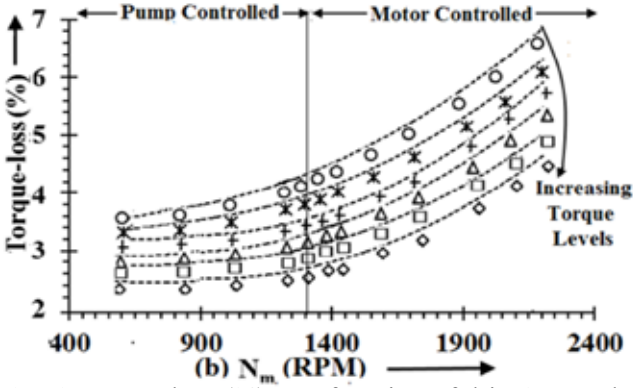

Fig. 6. Torque-loss (%) as a function of drive's speed

Table 3. Actual and theoretical values of the torque loss (%) of the drive at different loads.

T_{ld}=28 N m			T_{ld}=32 N m			T_{ld}=37 N m		
N_m (RPM)	Δt_{ta}	Δt_{tp}	N_m (RPM)	Δt_{ta}	Δt_{tp}	N_m (RPM)	Δt_{ta}	Δt_{tp}
601	2.3	2.4	607	2.6	2.7	601	2.8	3.0
844	2.4	2.4	853	2.7	2.8	844	2.9	3.0
1043	2.4	2.6	1030	2.8	2.9	1037	3.0	3.1
1236	2.5	2.7	1239	2.8	3.0	1233	3.1	3.2
1315	2.6	2.7	1315	2.9	3.1	1312	3.2	3.3
1391	2.7	2.8	1384	3.0	3.1	1387	3.3	3.4
1444	2.7	2.9	1447	3.1	3.2	1438	3.3	3.5
1596	3.0	3.1	1590	3.3	3.5	1586	3.7	3.8
1741	3.2	3.4	1732	3.6	3.8	1729	3.9	4.1
1956	3.8	3.9	1950	4.1	4.4	1937	4.4	4.7
2098	4.1	4.3	2098	4.5	4.8	2076	4.9	5.1
2215	4.5	4.7	2221	4.9	5.1	2215	5.4	5.5
2400	5.1	5.3	2400	5.5	5.8	2400	5.9	6.2
T_{ld}=42 N m			T_{ld}=46 N m			T_{ld}=50 N m		
N_m (RPM)	Δt_{ta}	Δt_{tp}	N_m (RPM)	Δt_{ta}	Δt_{tp}	N_m (RPM)	Δt_{ta}	Δt_{tp}
607	3.1	3.2	613	3.3	3.3	613	3.5	3.6
831	3.1	3.2	834	3.4	3.4	828	3.7	3.8
1027	3.2	3.4	1021	3.5	3.5	1011	3.8	4.0
1226	3.4	3.5	1226	3.7	3.7	1220	4.0	4.2
1308	3.5	3.6	1302	3.8	3.8	1286	4.1	4.3
1372	3.5	3.6	1359	3.9	3.9	1353	4.3	4.4
1428	3.6	3.7	1425	4.0	4.0	1413	4.4	4.6
1590	3.9	4.0	1564	4.3	4.3	1552	4.7	4.8
1713	4.2	4.4	1716	4.6	4.6	1688	5.0	5.1
1928	4.8	5.0	1912	5.2	5.2	1880	5.5	5.7
2067	5.3	5.4	2060	5.6	5.6	2019	6.0	6.2
2212	5.8	5.8	2203	6.1	6.1	2180	6.6	6.7
2400	6.3	6.5	2392	6.7	6.7	2367	7.2	7.4

2. At a constant speed, with a rise in load torque, the torque-loss percentage decreases. This is because Rvm increases with increasing load torque, as shown in Figures 3(c) and 4(c). The drag resistance Rpd also increases with a rise in load torque (3(d) and 4(d)). Therefore, moving towards the increasing torque levels, the percentage of torque loss decreases.

4.3 Overall performance of the drive

Drive efficiency depends on the slip and the torque-loss percentage. These are shown in Figures 5 and 6, respectively. The predicted overall efficiency given by Equation (13) (Appendix 1) is compared with the test-data obtained from Equation (12). The comparison between the test data and the predicted efficiency is shown in Figure 7. From Figure 7, it is evident that:

1. Drive efficiency in the pump-controlled mode of operation increases up to 1350 rpm due to an decrease in slip. Also, with a further increase in speed (above 1350 rpm) in motor-controlled mode, the slip predominates over the percentage of torque losses, leading to decreased drive efficiency.
2. The drive's efficiency in the motor controlled mode of operation starts decreasing with an increase in drive speed (above 1350 rpm). This is due to the fact that leakage resistances, R_{pl}

and R_{ml}, decrease (Figures 4(a) and 4(b)) with a decrease in the motor displacement ratio (β_{md}).

3. The drive's efficiency rises with an increase in the load torque at a constant speed. This is due to the fact that the percentage of torque-loss predominates over the slip of the drive, and it decreases with increasing torque levels at a particular speed, as given in Figure 6. Higher efficiency at a high load torque of the piston-type hydrostatic machine is also recognized by McCandlish *et al.* (1984), Mandal *et al.* (2009), and Thoma, (1969).

4. The highest efficiency of the pump-controlled HST drive is about 87%, whereas the maximum efficiency of the drive in the motor-controlled mode of operation is 84%, as shown in Figure 7. This is due to the fact that the slip of the drive in the pump-controlled mode of operation is less than that in the motor controlled mode.

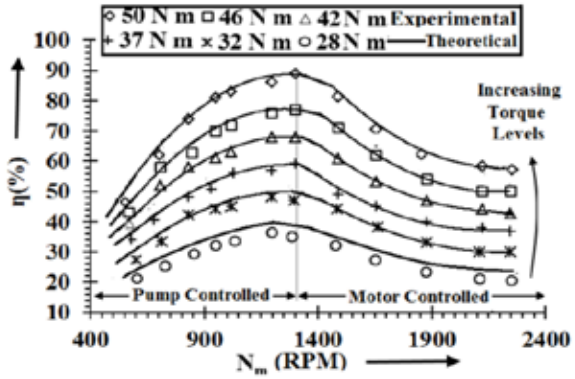

Fig. 7. Comparison of the predicted and actual drive's efficiency

Table 4. Actual and theoretical values. Overall efficiency of the drive at differenttorque loads.

T_{id}=28 N m			T_{id}=32 N m			T_{id}=37 N m		
N_m (RPM)	η_a(%)	η_t(%)	N_m (RPM)	η_a(%)	η_t(%)	N_m (RPM)	η_a(%)	η_t(%)
601	22	24	606	30	32	580	36	37
725	26	29	715	35	37	677	42	43
862	30	33	831	42	44	837	50	50
950	33	35	952	44	47	920	52	53
1033	34	37	1023	46	48	1023	56	56
1199	37	39	1196	49	50	1190	58	59
1288	37	39	1298	48	50	1298	60	61
1477	33	35	1491	45	45	1491	50	52
1649	28	31	1664	39	40	1657	46	46
1879	24	27	1875	33	34	1882	41	40
2104	22	24	2106	31	32	2126	38	39
2382	22	25	2376	31	32	2382	39	40
T_{id}=42 N m			T_{id}=46 N m			T_{id}=50 N m		
N_m (RPM)	η_a(%)	η_t(%)	N_m (RPM)	η_a(%)	η_t(%)	N_m (RPM)	η_a(%)	η_t(%)
574	41	42	570	44	45	556	48	50
721	52	53	717	58	59	703	62	64
837	58	59	843	63	65	829	74	75
946	61	62	948	70	71	955	81	81
1023	63	65	1017	72	73	1017	83	84
1196	68	69	1199	76	78	1199	85	88
1298	68	70	1304	77	78	1297	88	89
1484	61	62	1486	71	71	1493	82	83
1651	54	56	1654	62	63	1647	71	72
1869	47	50	1878	55	56	1857	63	64
2126	44	46	2123	50	51	2130	58	60
2388	43	45	2381	50	52	2388	59	60

From the above observations, it may be inferred that the pump-controlled HST drive is efficient for high torque and high speed ranges. In contrast, for high torque and low speed ranges, the motor-controlled drive was found to be more efficient. The variation in the theoretical and the actual efficiencies is about +1% to +3%. Various factors such as hydrodynamic losses, flow loss due to a thermal effect, bearing friction, other additional leakage paths, etc. were not considered in the present study. Consideration of the previous effects needs more detailed modelling, and it also requires the incorporation of statistical data.

5. Conclusions

In this article, the performance parameters of a closed-circuit hydrostatic drive have been investigated using bond graph simulation technique where torque and flow losses are accounted for by the resistive elements. The relationship of these resistances with system variables can be experimentally determined. They are found to have non-linear relationships with the torque and the displacements of the pump and the hydro-motor. Using them, the predicted performance parameters of the closed circuit HST drive are experimentally obtained and verified. Owing to the wide change in the operational conditions to recognize the non-linearity of the drive performance, the nature of the resistances are described by the quadratic relationship and found to be highly adaptable. They result in good correlations with experimental data. It is shown that when a simulated response of the model is combined with experimental observations, the result is a reduction of the effective load on the data handling. Comparing the test data with simulation results, the losses of the HST drives are estimated at running conditions. This may be difficult to perform in practice. For such loss estimation, the component does not need to be disassembled, and a special measurement technique is not required. The proposed method for predicting the performance may be useful to engineering application when selecting a similar drive system. The steady-state characteristics of the slip, torque-loss and overall efficiency of the proposed drive operating in fluctuating load conditions can be used to operate the system in pump-and motor-controlled modes. When switching over from pump to motor or control or vice-versa, it will be run through a suitable controller with respect to its variable load profile. The model is found to be highly adaptable and it agrees fairly well with the experimental data. This enhances the reusability of the model and improves its predictive power. Thus, a future study may be useful on the minimizing of power consumption and optimizing energy maintenance.

References

British Standards Institution (2007) 4409: Methods for determining the performance of pumps and motors for hydraulic fluid power transmission.

Conrad, F., Trostmann, E. & Zhang, M. (1993). Automatic computer controlled bi-directional dynamometer applied for identification of static performance and experimental modelling of losses in hydraulic pumps and

motors. In: 3rd Scandinavian International Conference on Fluid Power, Linköping, Sweden, 25-26: 1:25-36

Hasan, E., Dasgupta, K., & Ghoshal, S. (2017). Comparison of the efficiency of the high speed low torque hydrostatic drives using bent axis motor: An experimental study. Proceedings of the Institution of Mechanical Engineers, Part E: Journal of Process Mechanical Engineering, 231(4): 650–666.

Ivantysyn, J. & Ivantysynova, M. (2002). Hydrostatic pumps and motors. Tech Books International, 1st Ed., pp.448-471, New Delhi (India).

Kumar, N. & Dasgupta, K. (2015). Steady-state performance investigation of hydrostatic summation drives using bent-axis hydraulic motor. Proceedings of the Institution of Mechanical Engineers, Part C: Journal of Mechanical Engineering Science, 229(17): 3234-3255.

Khorshid, E., & Gad, O. (2006). Predicting the performance of an electrohydraulic servomotor using mathematical modelling and natural networks. Kuwait Journal of Science, 33(2):175-204

Kohmäscher, T., Rahmfeld, R. & Murrenhoff, H. (2007). Improved loss modelling of hydrostatic units: Requirement for precise simulation of mobile working machine drivelines, In: American Society of Mechanical Engineers. International Mechanical Engineering Congress and Exposition, Seattle, Washington (USA), Nov. 11-15. Paper no. IMECH2007-41803:195-206.

Lux, J. & Murrenhoff, H. (2016). Experimental loss analysis of displacement controlled pumps, In: 10th International Fluid Power Conference, Dresden, Germany. Paper no. I-2: 441-451.

Mandal, S.K., Dasgupta, K. & Pan, S.A (2009). Theoretical and experimental studies on the steady-state performance of low-speed high-torque hydrostatic drives in Part 1: Modelling. Proceedings of the Institution of Mechanical Engineers, Part C: Journal of Mechanical Engineering Science, 223(11): 2663-2674.

Mandal, S. K., Dasgupta, K. &. Pan, S. (2009). Theoretical and experimental studies on the steady-state performance of low-speed high-torque hydrostatic drive Part 2: experimental investigation. Proceedings of the Institution of Mechanical Engineers, Part C: Journal of Mechanical Engineering Science, 223(11): 2675-2685.

McCandlish, D. & Dorey, R. E. (1984). The mathematical modelling of the hydrostatic piston pumps and the motors. Proceedings of the Institution of Mechanical Engineers, Part B: Journal of Engineering Manufacture, 198(10): 165-174.

Ozfirat, K.M., Malli, T., Ozfirat, P.M., Kahraman, B. (2017). The performance prediction of roadheaders with response surface analysis for underground metal mine. Kuwait Journal of Science, 44(2): 112-120.

Rahmfeld, R. & Skirde, E. (2010). Efficiency measurement and modelling–essential for optimising hydrostatic systems. In:7th International Fluid Power Conference, Aachen, Germany, 2010, 2: 1-14.

Stojanovic, C., Bogdanovic, D., Urosevic, S. (2015). Selection of the optimal technology for surface mining by multi-criteria analysis. Kuwait Journal of Science, 42 (3): 170-190.

Thoma, J.U. (1969). Mathematical models and effective performance of hydrostatic machines and transmission. Hydraulic Pneumatic Power, 15: 642-651.

Thoma, J.U. (1990). Simulation by bondgraph, Berlin: Springer.pp. 57-71

Watton, J. (2006). An explicit design approach to determine the optimum steady-state performance of axial piston motor drives. Proceedings of the Institution of Mechanical Engineers, Part I: Journal of Systems and Control Engineering, 220(2): 131-143.

Watton, J. (2009). Fundamentals of fluid power control. Cambridge University Press: London, 1st Ed., pp.179-181.

Williamson, C. & Ivantysynova, M. (2007). The effect of pump efficiency on displacement-controlled actuator systems. In: Proceedings of the Tenth Scandinavian International Conference on Fluid Power, Tampere, Finland, 2: 301-326.

Zarotti, G.L. & Nervegna, N. (1983). Pump efficiencies, approximations and modelling. In: Proceeding of the Sixth International Symposium on Fluid power. Cambridge, England, Paper no. C3:145-164. Product catalogue of the variable displacement axial piston pump, RA 92003-A/06.09 Bosch Rexroth, Germany. Product catalogue of the variable displacement bent axis hydro-motor, RE 91001/09.00 Bosch Rexroth, Germany.

Submitted: 15-06-2017
Revised: 11-09-2017
Accepted: 08-10-2017

بحث عن أداء نظام هيدروستاتيكي مغلق الدائرة في الحالة المستقرة - نهج عملي

*أجيت كومار باندي ، ك. داسجوبتا، ن كومار

دانباد - 826004، جهارخاند، الهند ،(IIT (ISM ،قسم هندسة الآلات والتعدين

* ajit.saurabh100@gmail.com

الملخص

تدرس هذه المقالة أداء محرك هيدروستاتيكي (HST) من خلال النمذجة والتجربة. إن المحرك موضوع الدراسة المُستخدم للتحليل ذو دائرة مغلقة، حيث يؤدي الإمداد من مضخة الإزاحة المتغيرة إلى حركة هيدروليكية متغيرة الإزاحة. يهدف هذا البحث إلى إظهار التحكم في سرعة عزم الدوران في المحرك الهيدروستاتيكي، والذي يتحقق عن طريق تغيير المضخة أو إزاحة المحرك من حيث الكفاءة الكلية، ونسبة خسارة عزم الدوران (٪) والانزلاق. تم استخدام طريقة المحاكاة بالربط البياني لنمذجة المحرك الهيدروستاتيكي حيث تم تجميع مفقودات المضخة والمحرك الهيدروليكي من خلال المقاومات. وتم تحديد خصائص المفقودات من خلال اختبار البيانات. وتتمثل المساهمة الرئيسية لهذا البحث في دراسة أداء المحرك فيما يتعلق بتغير المضخة والتشريد الكهرومائي، والتي قد تكون مفيدة لمهندسي التصميم والمصنعين أثناء تنفيذ إرشادات التحكم الخاصة بالمحركات الهيدروستاتيكية المستخدمة في التعدين. ويحدد البحث منطقة التشغيل الفعالة للمحرك، والتي ستكون مفيدة في التطبيقات الهندسية.